NASA TECHNICAL NOTE

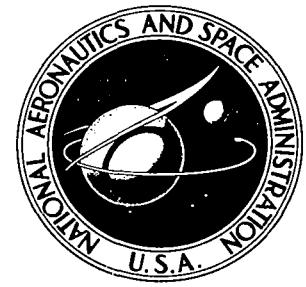

NASA TN D-6609

MATHEMATICAL MODEL OF WATER TRANSPORT IN BACON AND ALKALINE MATRIX-TYPE HYDROGEN-OXYGEN FUEL CELLS

by Paul R. Prokopius and Robert W. Easter

Lewis Research Center
Cleveland, Ohio 44135

NATIONAL AERONAUTICS AND SPACE ADMINISTRATION • WASHINGTON, D. C. • MARCH 1972

1. Report No.	2. Government Accession No.	3. Recipient's Catalog No.
NASA TN D-6609		

4. Title and Subtitle	5. Report Date
MATHEMATICAL MODEL OF WATER TRANSPORT IN BACON AND ALKALINE MATRIX-TYPE HYDROGEN-OXYGEN FUEL CELLS	March 1972
	6. Performing Organization Code

7. Author(s)	8. Performing Organization Report No.
Paul R. Prokopius and Robert W. Easter	E-6118
	10. Work Unit No. 113-34

9. Performing Organization Name and Address	11. Contract or Grant No.
Lewis Research Center National Aeronautics and Space Administration Cleveland, Ohio 44135	

12. Sponsoring Agency Name and Address	13. Type of Report and Period Covered
National Aeronautics and Space Administration Washington, D.C. 20546	Technical Note
	14. Sponsoring Agency Code

15. Supplementary Notes

16. Abstract

Based on general mass continuity and diffusive transport equations, a mathematical model was developed that simulates the transport of water in Bacon and alkaline-matrix fuel cells. The derived model was validated by using it to analytically reproduce various Bacon and matrix-cell experimental water transport transients.

17. Key Words (Suggested by Author(s))	18. Distribution Statement
Mathematical model Water transport Fuel cells	Unclassified - unlimited

19. Security Classif. (of this report)	20. Security Classif. (of this page)	21. No. of Pages	22. Price*
Unclassified	Unclassified	47	$3.00

* For sale by the National Technical Information Service, Springfield, Virginia 22151

CONTENTS

MATHEMATICAL MODEL OF WATER TRANSPORT IN BACON AND ALKALINE MATRIX-TYPE HYDROGEN-OXYGEN FUEL CELLS

by Paul R. Prokopius and Robert W. Easter

Lewis Research Center

SUMMARY

As part of a continuing program in the study of the water transport processes in hydrogen-oxygen fuel cells, a mathematical model was developed that simulates the transport in both Bacon and alkaline - matrix cells.

Aside from identifying and defining the processes controlling water transport in these two types of cells, the model appears to be sufficiently general to provide a basis for simulating the transport processes in other state-of-the-art fuel cells.

The model specifically identifies the basic water transport process in matrix cells to be higher than first order. This is significant in that the electrolyte drying which occurs following a matrix cell load increase can be partially attributed to this higher order characteristic and thus is not completely the result of operating temperature changes as is commonly believed.

The model was developed by applying the general laws of mass continuity and diffusive mass transfer to the transport zones in a lumped parameter mass transport analysis. The result is a simulation that comprises five simultaneous, nonlinear differential equations that predict the movement of both water and hydroxide ions within a cell.

Validation of the model was accomplished by comparing analytically obtained water transport data with corresponding data obtained in previously conducted experimental water transport studies.

INTRODUCTION

Control of the water inventory in the electrolyte of hydrogen-oxygen fuel cells is the prime requisite in maintaining cell electrolyte concentration within design limits and hence contributes to safe and efficient operation during both normal and emergency operating periods. The design of systems needed to achieve this type of control could

be greatly aided by an understanding of the mechanisms that regulate the movement and hence the rejection of product water from an operating cell. On this basis a program is being conducted at the Lewis Research Center to identify and mathematically simulate the processes controlling fuel-cell water transport for both steady-state and transient operation.

The water removal technique studied in this program is one in which the product water is evaporated into a circulating reactant (H_2) stream. The rate of evaporation is controlled by regulating the parameters, particularly the inlet humidity, of the circulating hydrogen stream.

As a first step in gaining an understanding of fuel-cell water transport, experimental and analytical studies of the water transport in a Bacon cell were conducted. The results of these studies are presented in reference 1. On completion of the Bacon cell work, the program emphasis was shifted to matrix cells, and an experimental dynamics study was conducted and reported on in reference 2. From the data obtained in this study, it became evident that the mathematical Bacon cell model lacked the generality to be applicable to a matrix cell. Therefore, using the theory developed in the Bacon cell model as a starting point, a model has been developed that is sufficiently general to simulate the water transport of both Bacon and alkaline matrix cells.

As in the case of the Bacon cell, this model was developed on a lumped parameter basis. The movement of water within the cell is simulated by applying the equation of continuity and the laws of diffusive transport to the various zones or lumps into which the cell structure was schematically divided.

The model equations were simulated on an analog computer on which the perturbations applied in the experimental water transport studies were reproduced analytically. By comparing the analytically obtained response data with the corresponding experimental data, the model was found to be a valid simulation of both the Bacon and matrix cell water transport. In addition, the model appears to be sufficiently general to serve as the nucleus for the transport simulation for cells that employ methods other than the circulating reactant water removal technique.

MODEL DEVELOPMENT

A schematic diagram of the cell for which the model was developed is shown in figure 1. The cell shown in this diagram is a matrix cell of the same type used in an experimental water-rejection dynamics test program previously conducted (ref. 2). In this cell the electrodes consist of a nickel screen coated with a mixture of platinum black catalyst and Teflon binder, and the electrolyte is an aqueous potassium hydroxide solution. The product water is evaporated from the electrolyte contained in the hydro-

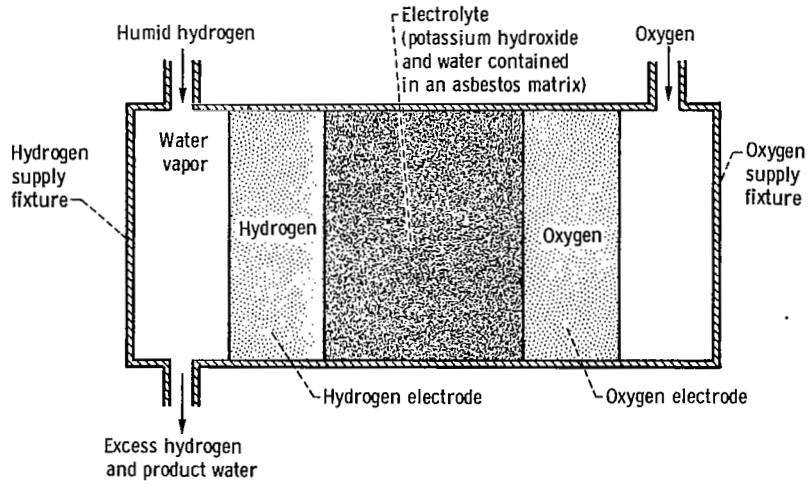

Figure 1. - Fuel cell.

gen electrode and removed from the cell by flowing a controlled excess of humid hydrogen through the hydrogen supply chamber.

The mass transport model that was developed is one dimensional. This characteristic is implicit in the macroscopic or lumped parameter analysis that was used in the derivation.

The model is analytical in all aspects except in the simulation of the effect that cell operating temperature has on the water-rejection process. In lieu of deriving a complete heat-transfer model to provide a totally analytical simulation, the thermal characteristics and their related effects on the water-rejection process were synthesized empirically when testing the validity of the analytical model on the analog computer; that is, for any particular perturbation, experimental cell-temperature response data were used to obtain a corresponding correction in electrolyte vapor pressure. Since the rate of water rejection is a function of the electrolyte vapor pressure, the thermal effects were accounted for by superimposing the temperature correction on the program-calculated vapor pressure.

Accounting for the temperature effect in this manner assumes that temperature gradients within the cell are negligible. This assumption was justified by experimental thermal response data taken during various load-step transients in which a negligible difference was observed between the temperatures of the reactant-side surfaces of the two electrodes.

The zones selected for deriving the model are depicted in schematic form in figure 2. The transport of water and OH ions that occurs within the electrode-matrix

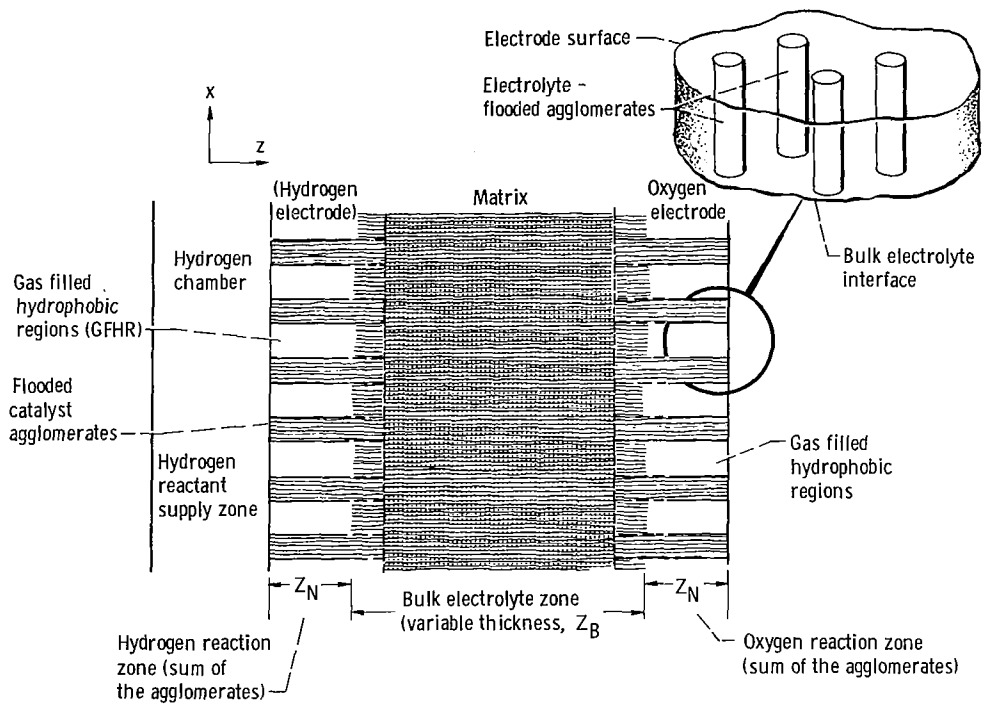

Figure 2. - Model schematic.

structure is included in the analysis, as is the rejection of water vapor into the hydrogen supply stream. The transport of water within the reactant chamber is considered to be at steady-state because the lag or retention time of water vapor within the chamber is negligible.

To represent the electrodes, a flooded agglomerate configuration is used (ref. 3). The theory proposed in the development of this electrode model states that the catalyst present in Teflon bonded platinum electrodes tends to form porous agglomerates that flood with electrolyte. The presence of Teflon creates hydrophobic gas filled regions that surround the agglomerates and provide passages for reactants to diffuse into the available catalyst reaction sites. In the case of the hydrogen electrode, these regions also provide a path for the evaporated product water to diffuse into the flowing hydrogen stream. To approximate the electrode geometry, the agglomerates can be considered to be electrolyte-filled cylinders that extend from the matrix to the gas-side surface of the electrode (see fig. 2). The electrolyte completely fills the matrix plus a portion of each electrode, thereby flooding not only the agglomerates, but also a portion of the void volume surrounding the agglomerates (subsequently referred to as the gas-filled hydrophobic regions, GFHR). Changes in electrolyte volume due to changes in electrolyte concentration are taken up by the gas-filled hydrophobic regions; the result being a variation in the flooded volume of each electrode. It is assumed that under all conditions

both electrodes are flooded by the same amount; that is, the ratio of filled to unfilled volume is equal.

Within the cell configuration depicted in figure 2, the four mass transport zones are

(1) The hydrogen supply chamber: this is the rectangularly shaped gas passage through which the humidified hydrogen stream is supplied to the cell

(2) The bulk electrolyte zone: this is composed of the volume of KOH-filled matrix plus the volume occupied by the KOH that floods into the originally gas-filled regions that surround the flooded electrode-agglomerates

(3) and (4) The hydrogen and oxygen reaction zones: these consist of the sum total of the volume occupied by the agglomerate cylinders that extend from the electrolyte-filled portion to the gas-side surface of each electrode.

The mathematical analysis is based on the continuity of water and hydroxide ions present in the zones described. The resulting mathematical simulation, the derivation of which is presented in detail in appendix A, is expressed by five nonlinear first-order differential equations.

The model equations, in the form in which they were programmed for solution on an analog computer, are the following continuity equations:

(1) Water in the hydrogen reaction zone

$$\frac{dM_{H_2O-H_2}}{dt} = 1.87\times10^{-7}(I) - CA_{Z-H_2}(\overline{P}^* - P_{s,i}) - \overline{D}_{H_2O-KOH}A_Z\left(\frac{\frac{M_{H_2O-H_2}}{V_{H_2}} - \frac{M_{H_2O-B}}{V_B}}{\frac{Z_B}{2}}\right) \tag{A20}$$

(2) Water in the bulk electrolyte zone

$$\frac{dM_{H_2O-B}}{dt} = \overline{D}_{H_2O-KOH}A_Z\left(\frac{\frac{M_{H_2O-H_2}}{V_{H_2}} - \frac{M_{H_2O-B}}{V_B}}{\frac{Z_B}{2}}\right) - D_{H_2O-KOH}A_Z\left(\frac{\frac{M_{H_2O-B}}{V_B} - \frac{M_{H_2O-O_2}}{V_{O_2}}}{\frac{Z_B}{2}}\right) \tag{A22}$$

(3) Water in the oxygen reaction zone

$$\frac{dM_{H_2O-O_2}}{dt} = \bar{D}_{H_2O-KOH} A_Z \left(\frac{\frac{M_{H_2O-B}}{V_B} - \frac{M_{H_2O-O_2}}{V_{O_2}}}{\frac{Z_B}{2}} \right) - 0.935\times10^{-7}(I) \qquad (A24)$$

(4) The hydroxide ions (OH^-) in the hydrogen reaction zone

$$\frac{dM_{OH^- - H_2}}{dt} = D' A_Z \left(\frac{\frac{M_{OH^- - B}}{V_B} - \frac{M_{OH^- - H_2}}{V_{H_2}}}{\frac{Z_B}{2}} \right) - 1.78\times10^{-7}(I) \qquad (A28)$$

(5) The hydroxide ions (OH^-) in the bulk electrolyte zone

$$\frac{dM_{OH^- - B}}{dt} = D' A_Z \left(\frac{\frac{M_{OH^- - O_2}}{V_{O_2}} - \frac{M_{OH^- - B}}{V_B}}{\frac{Z_B}{2}} \right) - D' A_Z \left(\frac{\frac{M_{OH^- - B}}{V_B} - \frac{M_{OH^- - H_2}}{V_{H_2}}}{\frac{Z_B}{2}} \right) \qquad (A29)$$

The symbols used in the preceding equations are defined in appendix B, and the values of the various cell parameters are presented in tabular form in the model derivation of appendix A.

The dependent variables in the model equations are the masses of water and OH^- present in the zones for which the respective continuity equations were written, and the independent variable is time. The mass flow expressions in the continuity equations are provided by applying Fick's law to the various model zones since the transport within the cell is diffusive in nature. The driving functions are the load current I and the partial pressure of the water vapor in the inlet-hydrogen stream $P_{s,i}$. The load current is a measure of the rate of water production, and the inlet stream vapor pressure is a measure of the water content or degree of humidification of the hydrogen stream.

Nonlinearities are present in the model because various cell parameters, which appear in the coefficients of these equations, are functions of the system dependent var-

iables, which, in this case, are the transport zone constituent masses; that is, parameters such as effective diffusivity, diffusion path length, and mass-transfer area are functions of the instantaneous electrolyte volume, which, in turn, is defined by the instantaneous mass makeup of the electrolyte in the various transport zones.

MODEL VERIFICATION

Verification of the mathematical model was accomplished by analytically reproducing experimentally obtained water-rejection response data. The verification consisted of comparing experimental data with the change in the rate of water rejection as measured by the term

$$(\dot{C})A_{Z\text{-}H_2}(\overline{P}^* - P_{s,i})$$

which appears in equation (A20). This expression actually represents the rate at which water is rejected from the hydrogen electrode into the hydrogen stream. However, by applying the assumption that no transport lag occurs in the gas chamber, this term can be used as a measure of the change in the flow rate of water exiting the cell and can then be compared with the water-rejection data obtained in the experimental study (ref. 2).

Both experimental and analytical data for a typical water-rejection response to a step in the rate of water production (load current) are shown in figure 3. In this figure the model correlates the experimental data to within 5 percent. It predicts the correct peaking and settling time of what is basically an underdamped second-order response, and it also approximates the slight ripple or higher-than-second-order characteristics that is superimposed on the basic second-order curve.

A typical model and experimental response correlation for a step in inlet stream humidity is shown in figure 4. Again, as for the power-step case, the maximum deviation between experimental and analytical data is less than 5 percent.

The changes in the experimentally observed responses caused by varying the amplitude of the input perturbation as well as the changes brought about by variations in pretransient operating conditions are also correctly predicted by the model.

The effect that the amplitude of the input step has on the water-rejection response is shown in figure 5. The curves of this figure are plots of normalized peak outlet water flow against load-step magnitude. Normalization was accomplished by dividing peak outlet water flow values by final (steady state) values. This was done for load current steps of several different magnitudes. The experimental curve, which was taken from the report on the matrix cell work (ref. 2), is compared with the corresponding analytical version obtained with the model.

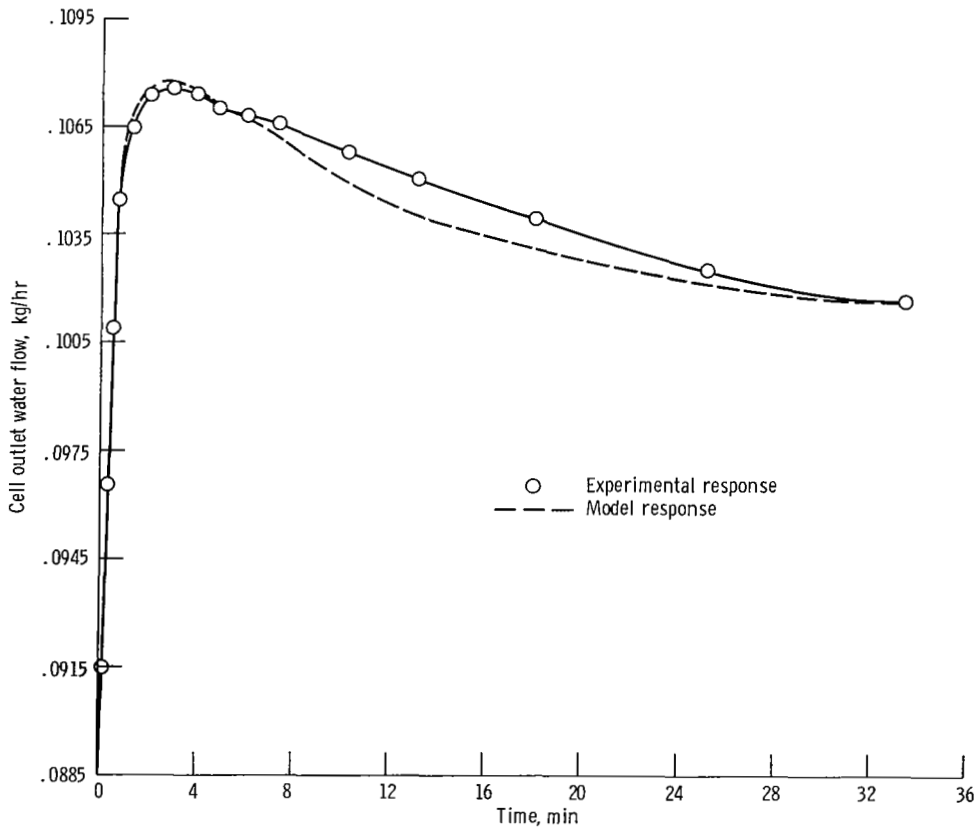

Figure 3. - Comparison of model and experimental outlet-stream water flow response to step in load current. Operating conditions: current step, 20 to 60 amperes; inlet stream hydrogen content 0.05 kilogram per hour (0.12 lb/hr); water content of inlet stream, 0.05 kilogram per hour (0.12 lb/hr).

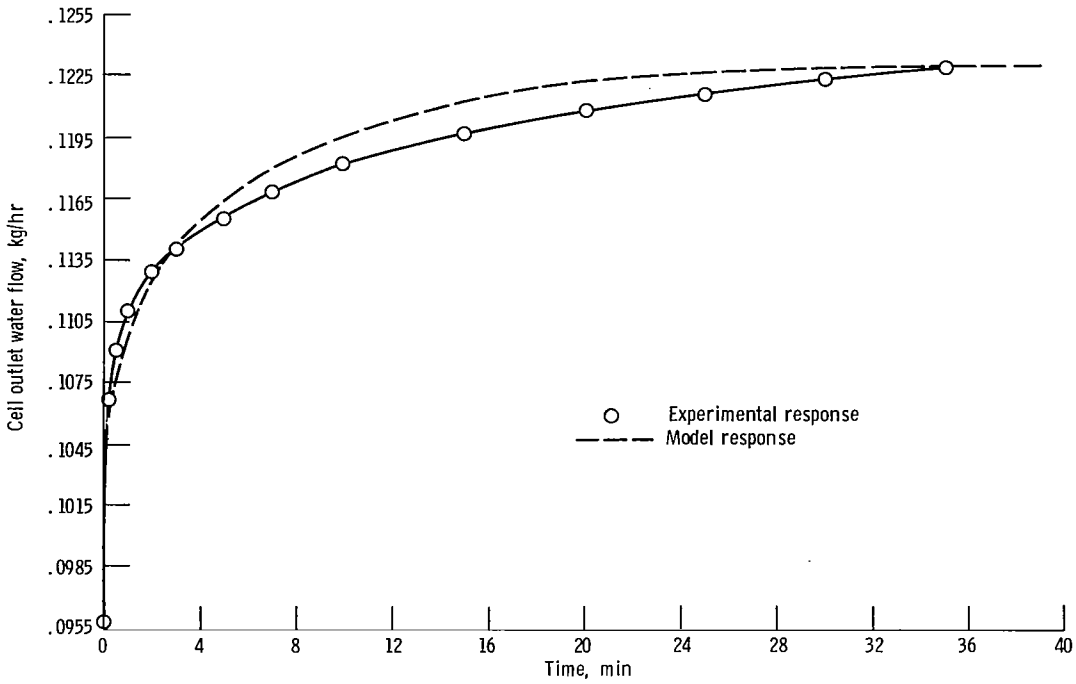

Figure 4. - Comparison of model and experimental outlet-stream water flow response to step in water content of the inlet hydrogen stream. Operating conditions: inlet-stream water content step, 0.082 to 0.11 kilogram per hour (0.18 to 0.24 lb/hr); inlet stream hydrogen content 0.05 kilogram per hour (0.12 lb/hr); load current. 41 amperes.

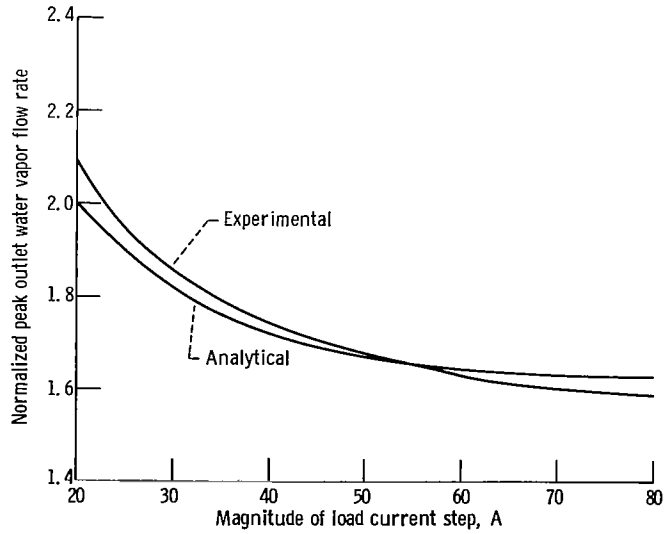

Figure 5. - Normalized peak outlet water flow rate as function of magnitude of load current step transient. Operating conditions: inlet-stream water content 0.082 kilogram per hour (0.18 lb/hr); inlet-stream hydrogen content, 0.05 kilogram per hour (0.12 lb/hr); initial load current, 20 amperes.

The plot of this peak-to-final ratio against current step magnitude identifies the water-rejection process for steps in cell current as being nonlinear (a linear process would result in a straight line). The close agreement between the curves of figure 5 indicates that the model correctly predicts this system nonlinearity.

Typical of the changes in response caused by variations in initial or prestep operating conditions are the data shown in figure 6(a). The two curves in this figure are responses to the same size power step taken at two different prestep inlet stream humidities. Since the prestep values and final steady-state water outflow values for the two differ from each other, the data are plotted on a normalized or percent-change basis to allow a direct comparison and to illustrate the response difference between the curves. The curves in figure 6(a) show that, as the inlet humidity is increased, the response overshoot decreases. The model simulates this same effect as seen from the data plotted in figure 6(b).

This response deviation is revealed by the model to be the result of system nonlinearities that stem from two matrix cell characteristics. These characteristics, which are discussed at greater length in appendix A, are the inlet hydrogen stream dependency of the electrode agglomerate mass-transfer area and the relative amount of electrolyte in the electrodes and matrix (see fig. 2). In the model these characteristics are translated into coefficients that are functions of the dependent variables and produce the nonlinear results.

To determine whether this water-transport simulation is general enough to predict the basic response characteristics of a Bacon cell, the model was adjusted to describe the Bacon cell used in the earlier water-rejection study (ref. 1), and several of the experimental perturbations were simulated. The adjustments that were made entailed changes in operating conditions, geometric parameters, and defining cell characteristics. The transport processes that are modeled were not changed, and thus the basic simulation remained intact.

An example of the type of cell characteristics taken into account is the difference between the "simple pore" configuration that represents the dual-porosity, sintered-nickel Bacon cell electrodes and the "flooded agglomerate" concept that simulates the Teflon bonded platinum catalyst electrodes of the matrix cell. In the model this difference was accounted for in the hydrogen reaction zone mass-transfer area. The mass-transfer area for the Bacon cell is merely the surface area of the electrode, while for the matrix cell it is the sum total of the cylindrical surface areas of the agglomerates in the nonflooded portion of the electrode.

A typical Bacon cell experimental response to a step in load current or the rate of water production along with the corresponding model response curve are shown in figure 7. Again, as for the matrix cell, the experimental and analytical response data are in good agreement.

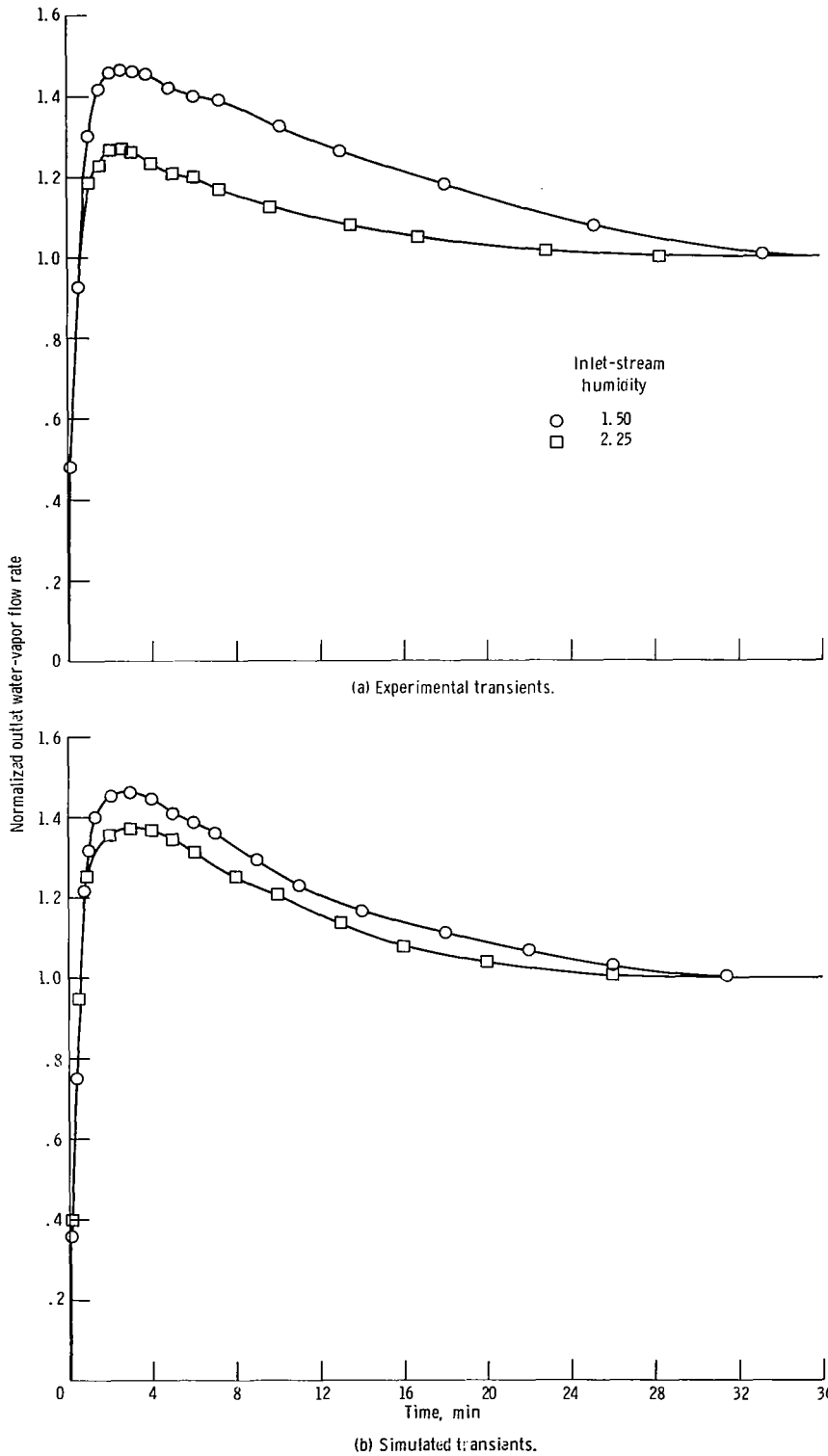

Figure 6. - Illustration of the effect that the magnitude of the inlet-stream humidity has on the outlet water-flow response to a step increase in cell load current. Operating conditions: current step 20 to 60 amperes; inlet-stream hydrogen flow, 0.05 kilogram per hour (0.12 lb/hr).

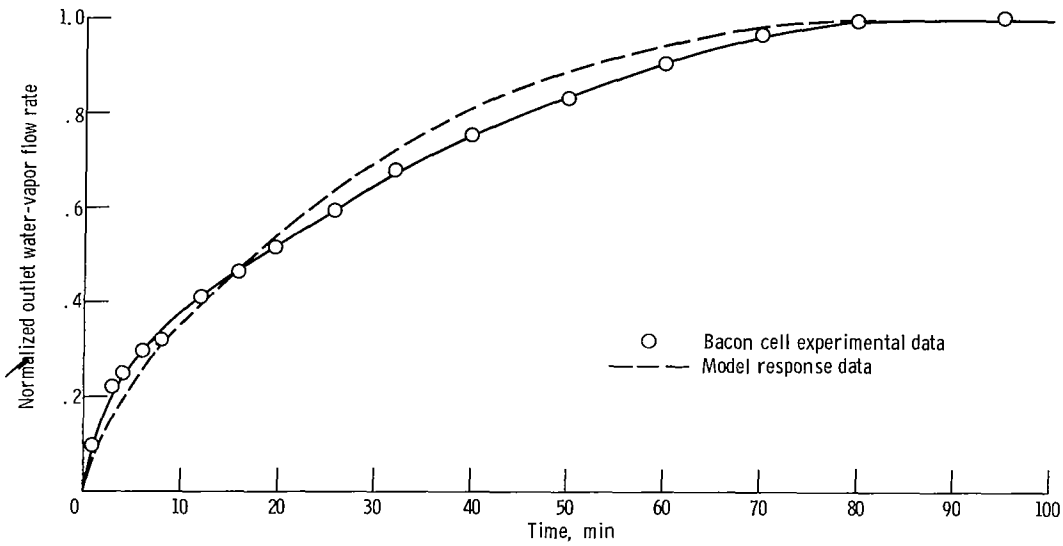

Figure 7. - Comparison of model and experimental Bacon cell outlet stream water flow response to a step in load current. Operating conditions: current step, 10 to 15 amperes; inlet stream dry hydrogen at 0.0058 kilogram per hour (0.0128 lb/hr).

Thus, since the model reproduces the basic response curves of both types of experimental transients for both cells plus all the various operating effects and system nonlinearities, it is concluded that it is a good generalized approximation of the water transport in Bacon and matrix cells which employ circulating reactant-stream water removal.

DISCUSSION

The basic response characteristics for both types of experimental steps for both cells were reproduced analytically as were all the various operating effects and system nonlinearities. Since this was accomplished, the validity of the model is established even though it was necessary to make approximations in sizing various undefined cell parameters such as the electrode and matrix tortuosity, the OH^- ion transport coefficient, and the radii of the cylindrical electrode agglomerates. The "curve fitting" latitude provided by these approximations might be sufficient to reproduce a single transient; however, it is obviously not sufficient to reproduce all the response characteristics.

An interesting matrix cell characteristic predicted by the model is that the water-rejection overshoot or drying evidenced by the load-step data cannot be totally attributed to a thermal effect; that is, the effect in which a cell temperature rise produced by a load step increases the electrolyte vapor pressure, which, in turn, causes water to be driven from the cell. Rather, the drying that occurs is, in part, the result of an inher-

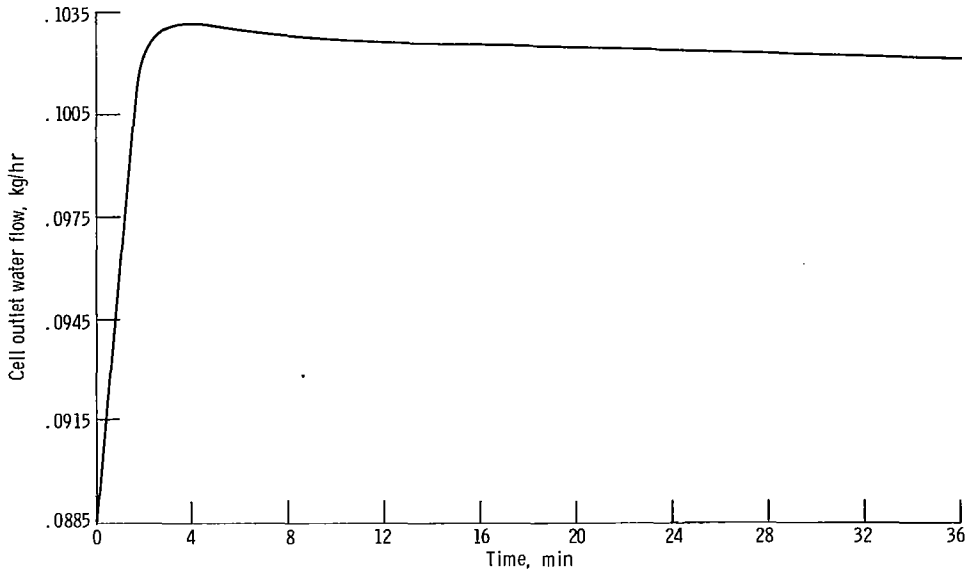

Figure 8. - Model outlet-stream water flow response to step in load current with cell operating isothermally. Operating conditions: current step, 20 to 60 amperes; inlet stream hydrogen content 0.05 kilogram per hour (0.12 lb/hr); water content of inlet stream, kilogram per hour (0.12 lb/hr).

ent characteristic of the cell. This is illustrated in figure 8 which is the model response for the load step shown in figure 3 with the temperature effects left out. The overshoot or drying effect, though not of the correct magnitude, is still present. This indicates that the basic transport process in a matrix cell is a higher-than-first-order phenomenon, an important fact when determining the characteristics of a system to control the water inventory for this type of cell.

A possible physical explanation is that the higher-than-first-order characteristic results from an imbalance in the diffusive resistance that exists across the cell structure. A step increase in load current produces an increase in the rate of water generation at the anode and an increase, one-half as large, in the rate of consumption at the cathode. If, as in the model, the resistance to water transport through the bulk electrolyte toward the cathode is higher than it is from the hydrogen reaction zone into the gas stream, the cell would have a tendency to reject more than one-half of the amount being generated at the anode. To satisfy the increased cathodic demand, water would be withdrawn from the bulk reservoir; the end result being on the reestablishment of equilibrium, a net removal of water from the cell.

In regards to generality or applicability to other types of cells, it is believed that the model could be used as a basis from which various additions or deletions would be made to account for differences between the type of cells modeled and the particular cell in question. Such additions to the existing model could represent such characteristics as a sizeable thermal gradient caused by liquid cooling, or the concentration gradients that accompany a static water removal system.

CONCLUSIONS

From the development of the mathematical water-transport model the following conclusions can be drawn:

1. A generalized mathematical simulation was developed for the water transport in Bacon and matrix cells that employ circulating reactant stream water removal. The validity of the model was established by the fact that it analytically reproduces both the linear and nonlinear transient response characteristics of both types of cells.

2. A matrix cell characteristic predicted by the model is that the basic transport, exclusive of operating temperature effects, is a higher-than-first-order process. The significance of this is that the electrolyte drying that accompanies a matrix cell load increase can be partially attributed to this higher-order effect and would thus be present to some degree even if the cell temperature were held constant during transient operation.

Lewis Research Center,
National Aeronautics and Space Administration,
Cleveland, Ohio, September 27, 1971,
113-34.

APPENDIX A

DERIVATION OF THE MATHEMATICAL MODEL

The electrochemical reaction at the anode

$$H_2 + 2OH^- \rightarrow 2H_2O + 2e^-$$

dictates that for every mole of hydrogen reactant consumed by the cell, two moles of water are formed. At steady state, one mole of product water must be rejected from the cell, and one mole is transported across the cell to be consumed in the overall cathodic reaction which is

$$\frac{O_2}{2} + H_2O + 2e^- \rightarrow 2OH^-$$

The hydroxide ions, which are the product of this reaction, are, in turn, transported to the hydrogen electrode for consumption in the anode reaction.

To simulate the cell mass transport that occurs during steady-state and transient operation, the continuity (mass conservation) equation was applied, on a lumped parameter basis, to the hydrogen, oxygen, and bulk transport zones defined in figure 2.

CONTINUITY EQUATION FOR WATER IN THE HYDROGEN REACTION ZONE

The continuity equation for water in the hydrogen reaction zone volume states that the rate of mass accumulation equals the rate of mass generation minus the rate of outflow. The equation can be expressed as

$$\frac{dM_{H_2O\text{-}H_2}}{dt} = w_R - w_S - w_{E\text{-}H_2} \tag{A1}$$

where w_R represents the generation rate w_S the mass outflow from the reaction zone into the hydrogen stream, and $w_{E\text{-}H_2}$ the outflow into the bulk electrolyte zone.

Inherent in a zonal or lumped parameter analysis such as this is the assumption that there are no gradients in the variables or cell parameters of any transport zone.

Rather, each parameter or variable within a zone is defined by an average value which is assumed to extend throughout that zone. In terms of the analysis, this states that the transport dynamic effects internal to the various zones are neglected.

DERIVATION OF RATE EXPRESSION FOR FLOW OF WATER VAPOR INTO HYDROGEN STREAM

The first of the rate terms to be derived will be w_S, since it depends to a higher degree on the details of the particular cell under consideration than do w_R and $w_{E\text{-}H_2}$ This sensitivity to cell detail plus the fact that it is necessary to describe w_S quite accurately to obtain satisfactory agreement with experiment make it impossible to derive a single, completely general expression for w_S. It will be shown, however, that cells of quite different character can, in many cases, be described by the same expression for w_S. In any case, a minimum amount of response data is needed to decide upon a specific form of w_S.

In the next section two expressions for N_{H_2O} will be considered in the light of the flooded agglomerate model geometry, where N_{H_2O} is the (local) flow rate of H_2O vapor out of the electrode per unit electrode geometric area. The first expression pertains if transport of water vapor in the gas-filled hydrophobic regions (GFHR) of the anode is controlled by a resistance associated with the liquid-gas interface. The second expression pertains if vapor phase diffusion in the z direction (perpendicular to the electrode surface) controls transport. Both expressions turn out to have the form

$$N_{H_2O} = h(P^* - P_s)$$

where P^* is the local (x-dependent) electrolyte equilibrium vapor pressure and P_s is the corresponding local H_2O partial pressure in the bulk gas phase in the gas cavity. Note that P^* is the mean vapor pressure over the z-direction. The parameters appearing in h, the local mass-transfer coefficient, differ according to which resistance is controlling.

Next, three possible distributions of N_{H_2O} and P^* over the face of the electrode will be considered. The first represents one extreme - that of constant (i.e., position independent) N_{H_2O}, where P^* is constant and the gas in the gas cavity is perfectly mixed. The second case is a condition of maximum variation of N_{H_2O}. Here, too, P^* is constant, but the bulk gas is in plug flow. The second case may be contrasted with

the third, wherein the bulk gas is in plug flow but the vapor pressure P^* varies with the stream partial pressure P_s such that $d/dx\,(P^* - P_s) = 0$, where x is the flow-path directed distance from the cell gas inlet.

All three cases yield expressions of the form

$$\frac{\tilde{w}_s}{\tilde{w}_T} = \psi(u)\frac{1}{\Pi}\left(\overline{P}^* - P_{s,i}\right)$$

where $\psi(u)$ is a dimensionless overall mass-transfer coefficient, Π is the mean total pressure in the gas cavity, $\overline{P}^*$ is the overall mean equilibrium vapor pressure, $P_{s,i}$ is the partial pressure of H_2O in the gas stream entering the cell, and $\tilde{w}_T$ is the total molar flow of gas into the cell (note that strictly speaking the forms of w_s to be derived apply only to cells in which product water is removed by excess hydrogen flow. So-called static water removal methods may, of course, be treated similarly but would yield somewhat different forms for w_s).

The dimensionless quantity u is given by

$$u = \frac{hA_Z}{\frac{\tilde{w}_T}{\Pi}}$$

where A_Z is the geometric electrode area. The three different cases mentioned previously yield different functional dependencies of ψ on u.

Finally, in the section Form of the Rate Expression the similarities and differences in the various resulting expressions will be discussed briefly, as will be the process by which one may arrive at a form applicable in a given situation. The form adopted for the simulation of the data given in reference 2 will be used as an example.

Water Vapor Transport in the Gas-Filled Hydrophobic Regions

Conservation of H_2O vapor in a differential volume of the GFHR yields

$$\frac{dN'_{H_2O}}{dZ'} = N_i\frac{\theta}{\varphi} \tag{A2}$$

where the accumulation of H_2O vapor and net transport in directions other than perpendicular to the electrode surface (the Z'-direction) is neglected. In equation (A2)

N_{H_2O} is the molar flux of H_2O in the gas-filled hydrophobic region in the Z' direction - the direction parallel to the axes of the agglomerates and towards the gas cavity; N_i is the molar rate of H_2O transport across a unit area of gas-liquid interface or agglomerate surface; θ is the interfacial area per unit electrode geometric volume; and φ is the gas-filled cross sectional area in the Z'-direction per unit electrode geometric surface area. Both θ and φ may be assumed to be independent of Z in accord with the flooded agglomerate model configuration.

Interfacial resistance controlling. - The chief transport resistance is postulated to be associated with the gas liquid interface. From this point of view the following assumptions are made:

(1) There are no Z'-direction H_2O concentration gradients in the liquid or gas phase. Thus, $P_{H_2O}(Z) = P_s$ for all Z', where P_s is the partial pressure of H_2O in the gas cavity immediately above the portion of electrode under consideration.

(2) The molar flux N_i is given by

$$N_i = k_i\left[P^* - P_{H_2O}(Z')\right] = k_i(P^* - P_s)$$

where k_i is the mass-transfer coefficient associated with the local gas-liquid interface and P^* is the equilibrium H_2O vapor pressure associated with the local liquid phase.

(3) All H_2O evaporates from the lateral surfaces of the agglomerates. Thus, $N'_{H_2O} = 0$ at $Z' = 0$ (the base of the agglomerates).

Introducing these assumptions into equation (A2) yields

$$\frac{dN'_{H_2O}}{dZ'} = \frac{\theta}{\varphi} k_i(P^* - P_s)$$

Integrating and applying assumption (3) yield

$$N'_{H_2O} = \frac{\theta}{\varphi} k_i(P^* - P_s)Z'$$

The rate of H_2O flow into the gas cavity per unit electrode geometric area N_{H_2O} is given by

$$N_{H_2O} = \varphi N'_{H_2O}\Big|_{Z'=Z_H} = \theta k_i Z_H(P^* - P_s) \qquad \text{(A3)}$$

where Z_H is the nonflooded agglomerate height.

Vapor diffusion controlling. - Here the transport resistance is postulated to be the Z-direction diffusion of water vapor. The following assumptions are made:

(1) The molar flux N_i is constant over the entire gas-liquid interface area; that is, N_i is independent of Z'.

(2) The molar flux N'_{H_2O} results from equimolar countercurrent diffusion (i.e., there is an equal but oppositely directed flux of hydrogen). Thus,

$$N'_{H_2O} = -\frac{D_g}{RT}\frac{P_{H_2O}(Z)}{dZ'} \tag{A4}$$

where D_g is the binary diffusion coefficient for H_2O - H_2, R is the gas constant, and T the absolute temperature.

(3) The molar flux N'_{H_2O} is zero at $Z' = 0$.

Applying these assumptions to equation (A2) and integrating twice yield (recalling that $P_{H_2O}(Z) = P_s$ at $Z' = Z_H$)

$$P_{H_2O}(Z) - P_s = \frac{N_i \theta RT}{2\varphi D_g}\left(Z_H^2 - Z'^2\right) \tag{A5}$$

Since in this approach the controlling transport resistance is Z-direction diffusion, the H_2O vapor in the GFHR may be considered to be in equilibrium with the surrounding liquid. Thus the mean partial pressure of H_2O vapor in the GFHR may be identified with the mean vapor pressure of the liquid in the local agglomerates. Mathematically,

$$P^* = \overline{P}_{H_2O}(Z) \equiv \frac{1}{Z_H}\int_0^{Z_H} P_{H_2O}(Z)\, dZ'$$

Thus,

$$P^* = P_s + \frac{N_i \theta RT}{3\varphi D_g} Z_H^2$$

This result may be solved for N_i, which then may be eliminated from equation (A5).

The flux N_{H_2O} may now be obtained from diffentiating the resulting expression:

$$N_{H_2O} = \varphi N'_{H_2O}\Big|_{Z'=Z_H} = -\frac{\varphi D_g}{RT}\frac{dP_{H_2O}}{dZ'}\Big|_{Z'=Z_H}$$

Thus

$$N_{H_2O} = \frac{3D_g\varphi}{RTZ_H}(P^* - P_s) \tag{A6}$$

Alternate expressions are now available for N_{H_2O}, the assumption of interface controlled transport leading to equation (A3) and the assumption of diffusion limited transport yielding equation (A6). Note that the driving force is the same but that the form of the coefficient differs. To summarize

$$N_{H_2O} = h(P^* - P_s) \tag{A7}$$

with

$$h \equiv h_1 = \theta k_i Z_H \quad \text{for interface control}$$

or

$$h \equiv h_2 = \frac{3D_g\varphi}{RTZ_H} \quad \text{for diffusion control}$$

where in either case h may be thought of as a local mass-transfer coefficient.

Distributions of Local Mass Flux and Vapor Pressure

In the preceding sections, care was taken to use the modifier "local" when discussing the quantities appearing in the expressions for N_{H_2O}. Indeed, N_{H_2O} and P^* may vary from place to place on the electrode, depending in a complicated way on such things as current density, temperature, and gas cavity partial pressure distributions. It is beyond the scope of this study to consider such dependency in detail. Rather, three representative cases will be postulated, which represent the spectrum of possible variation in N_{H_2O} and P^*: (a) N_{H_2O} and P^* independent of position, (b) maximum varia-

tion in N_{H_2O}, and (c) maximum variation in P^*.

Case (a) may be associated with a condition of maximum or "perfect" mixing in the bulk gas phase in the gas cavity. "Perfect mixing" is a commonly used term referring to a condition where there are no concentration gradients and where the outlet stream or streams are identical in composition to the gas in the gas cavity.

Cases (b) and (c), on the other hand, may be associated with a condition of minimum mixing or plug flow in the gas cavity. The term "plug flow" refers to a situation in which there is a definite direction (e.g., the X direction) to the flow and in which there is no mixing in the flow direction. Plug flow, then, yields the largest possible partial pressure gradients in the gas cavity. (For further discussion and examples of use of these mixing models see any text on chemical reactor design (e.g., ref. 4).)

The type of flow actually present in a given cell depends, of course, on the design of the gas cavity. Thus in some cases, it will be clear which type of flow exists. But even when the type of flow is not clear, one of the cases considered should be sufficient to describe the dynamic behavior of the cell since it will be seen that the resulting expressions for $\tilde{w}_s$ are quite similar. And under some conditions $\tilde{w}_s$ will be the same irrespective of the type of flow.

Case a: flux and vapor pressure independent of position (perfect mixing). - The general relation between $\tilde{w}_s$ and N_{H_2O} is

$$\tilde{w}_s = \int_{A_Z} N_{H_2O}\, dA \tag{A8}$$

where dA is an increment of electrode surface area and A_Z is the entire electrode surface area. Assuming that h in equation (A7) is independent of position and incorporating the perfect mixing characteristic (constant P_s), equation (A8) may be integrated in the perfect mixing case to give

$$\tilde{w}_s = hA_Z(\overline{P}^* - P_s) \tag{A9}$$

where

$$\overline{P}^* = \frac{1}{A_Z} \int_{A_Z} P^*\, dA$$

that is, $\overline{P}^*$ is the overall mean vapor pressure associated with the reaction zone - the quantity needed for the complete lumped parameter model.

It remains to eliminate P_s from the expression for w_s. This can be accomplished by means of the equation for conservation of H_2O vapor in the gas cavity. Neglecting the accumulation term results in

$$\tilde{w}^{in}_{H_2O} + \tilde{w}_s = \tilde{w}^{out}_{H_2O}$$

where the $\tilde{w}_{H_2O}$'s are molar flow rates. (It may be shown, with an order-of-magnitude analysis, that the accumulation term is generally negligible because of the very small residence times associated with the flowing stream.)

The molar flows may be related to partial pressures by the relations

$$\tilde{w}^{in}_{H_2O} = \frac{P_{s,i}}{\Pi} \tilde{w}_T$$

and

$$\tilde{w}^{out}_{H_2O} = \frac{P_s}{\Pi} \tilde{w}_T$$

where $\tilde{w}_T$ is the total molar flow rate through the cell and Π is the total pressure. Both $\tilde{w}_T$ and Π generally vary only slightly from inlet to outlet, so $\tilde{w}_T/\Pi$ may be assumed constant. Note that the expression for $\tilde{w}^{out}_{H_2O}$ includes the perfect mixing characteristic that $P^{out}_{H_2O} = P_s$.

Combining these relations with the expression for w_s yields

$$\frac{P_{s,i}}{\Pi} \tilde{w}_T + hA_Z(\overline{P}^* - P_s) = \frac{P_s}{\Pi} \tilde{w}_T$$

This may be solved for P_s:

$$P_s = \overline{P}^* - \frac{\frac{\tilde{w}_T}{\Pi}}{\frac{\tilde{w}_T}{\Pi} + hA_Z}$$

And this expression may be substituted into equation (A9) to yield

$$\frac{\tilde{w}_S}{\frac{\tilde{w}_T}{\Pi}} = \frac{u}{1+u}\left(\overline{P}^* - P_{S,i}\right) \tag{A10}$$

where

$$u = \frac{hA_Z}{\frac{\tilde{w}_T}{\Pi}}$$

Note that equation (A10) is of the form

$$\frac{\tilde{w}_S}{\frac{\tilde{w}_T}{\Pi}} = \psi(u)\left(\overline{P}^* - P_{S,i}\right)$$

where ψ may be thought of as a dimensionless overall mass-transfer coefficient.

Case b: maximum variation in flux (plug flow with constant vapor pressure). - Plug flow is characterized by the fact that no element of the fluid overtakes another element; that is, there is no mixing of the fluid in the direction of flow, although there may be mixing in the lateral direction.

If flow is in the X direction, a H_2O vapor mass balance on a differential volume element of the gas cavity yields

$$\frac{d\tilde{w}_{H_2O}}{dX} = N_{H_2O}\,l$$

where $\tilde{w}_{H_2O}$ is the molar flow of H_2O vapor and l is flow path width. Note that the accumulation term is neglected.

The molar flow may be related to the partial pressure by

$$\tilde{w}_{H_2O} = P_S \frac{\tilde{w}_T}{\Pi}$$

where $\tilde{w}_T/\Pi$ may again be assumed constant.

Substituting this relation and the general form of N_{H_2O} (eq. (A7)) into the mass balance yields

$$\frac{dP_s}{dX} = \frac{\Pi \ell h}{\tilde{w}_T} (P^* - P_s) \tag{A11}$$

This relation is characteristic of the plug flow condition.

The position dependency of P^* must now be introduced into equation (A11). It may be shown that the variation in N_{H_2O} is maximized, subject to the constraints that N_{H_2O} and dP^*/dX be zero or positive, if P^* is constant (these constraints arise from practical fuel cell operating requirements). Thus, for maximum variation in N_{H_2O} with position, the solution to equation (A11) is

$$P_s = P^* - (P^* - P_{s,i}) \exp\left(- \frac{h\ell}{\frac{\tilde{w}_T}{\Pi}} \right)$$

which employs the boundary condition that $P_s = P_{s,i}$ at $X = 0$.

Substitution of this expression for P_s into the expression for N_{H_2O} (eq. (A7)) gives N_{H_2O} with maximum position dependency.

The general relation between $\tilde{w}_s$ and N_{H_2O} (eq. (A8)) may now be integrated for this particular form of N_{H_2O} with the result that

$$\frac{\tilde{w}_s}{\frac{\tilde{w}_T}{\Pi}} = (1 - e^{-u})(P^* - P_{s,i}) \tag{A12}$$

where, again,

$$u = \frac{hA_Z}{\frac{\tilde{w}_T}{\Pi}}$$

and the expression for w_s is of the form

$$\frac{\tilde{w}_s}{\frac{\tilde{w}_T}{\Pi}} = \psi(u)(\overline{P}^* - P_{s,i})$$

Case c: maximum variation in vapor pressure (plug flow with constant flux). - In this case the flux N_{H_2O} is to remain constant, and the flow in the gas cavity is plug flow. Equivalently, $d(P^* - P_s)/dx$ is zero.

Equation (A11) again pertains; in this case the right hand side is constant, and so integration yields

$$P_s = P_{s,i} + \frac{\Pi \ell h}{\tilde{w}_T}(P^* - P_s)X$$

At the same time equation (A8) may be integrated for constant N_{H_2O} to give

$$\tilde{w}_s = N_{H_2O} A_Z = \ell L h(P^* - P_s) \qquad \text{(A13)}$$

where L is the flow path length.

Combining these two expressions yields

$$P_s = P_{s,i} + \frac{\Pi \tilde{w}_s}{\tilde{w}_T}\frac{X}{L}$$

Since it is desired to express $\tilde{w}_s$ in terms of $\overline{P}^*$, the constancy of N_{H_2O} in this case may be taken advantage of to write equation (A13) as

$$\tilde{w}_s = A_Z h(\overline{P}^* - \overline{P}_s)$$

The expression for P_s may be integrated to yield $\overline{P}_s$:

$$\overline{P}_s = P_{s,i} + \frac{1}{2}\frac{\Pi \tilde{w}_s}{\tilde{w}_T}$$

These two expressions may be combined to eliminate $\overline{P}_s$ and may be solved for $\tilde{w}_s$ to give

$$\frac{\frac{\tilde{w}_s}{\tilde{w}_T}}{\Pi} = \frac{u}{1 + \frac{u}{2}} (\bar{P}^* - P_{s,i}) \tag{A14}$$

where once again

$$u = \frac{\frac{hA_Z}{\tilde{w}_T}}{\Pi}$$

and the relation again is of the form

$$\frac{\frac{\tilde{w}_s}{\tilde{w}_T}}{\Pi} = \psi(u)(\bar{P}^* - P_{s,i})$$

Form of the Rate Expression

It has been seen that all the cases considered in the preceding section yield the same type of expression for w_s, namely,

$$\frac{\frac{\tilde{w}_s}{\tilde{w}_T}}{\Pi} = \psi(u)(\bar{P}^* - P_{s,i})$$

with

$$u = \frac{\frac{hA_Z}{\tilde{w}_T}}{\Pi}$$

From the section Water Vapor Transport in Gas-Filled Hydrophobic Region, the alternatives for h are

$$h \equiv h_1 = \theta k_i Z_H \quad \text{for interface control}$$

$$h \equiv h_2 = \frac{3D_g \varphi}{RTZ_H} \quad \text{for diffusion control}$$

And from the section Distributions of Local Mass Flux and Vapor Pressure, the three alternatives for $\psi(u)$ are

$$\psi(u) \equiv \psi_1 = \frac{u}{1+u} \tag{A10}$$

$$\psi(u) \equiv \psi_2 = 1 - e^{-u} \tag{A12}$$

$$\psi(u) \equiv \psi_3 = \frac{u}{1+\frac{u}{2}} \tag{A14}$$

Figure 9 shows the behavior of ψ_1, ψ_2, and ψ_3 over several decades of u values.

The first property common to the ψ's, regardless of functional form, is that they are monotonic with u and, hence, with h. This makes it possible to determine from a small amount of experimental data which type of transport takes place in the GFHR, that is, which form of h (h_1 or h_2) is applicable to a particular fuel cell.

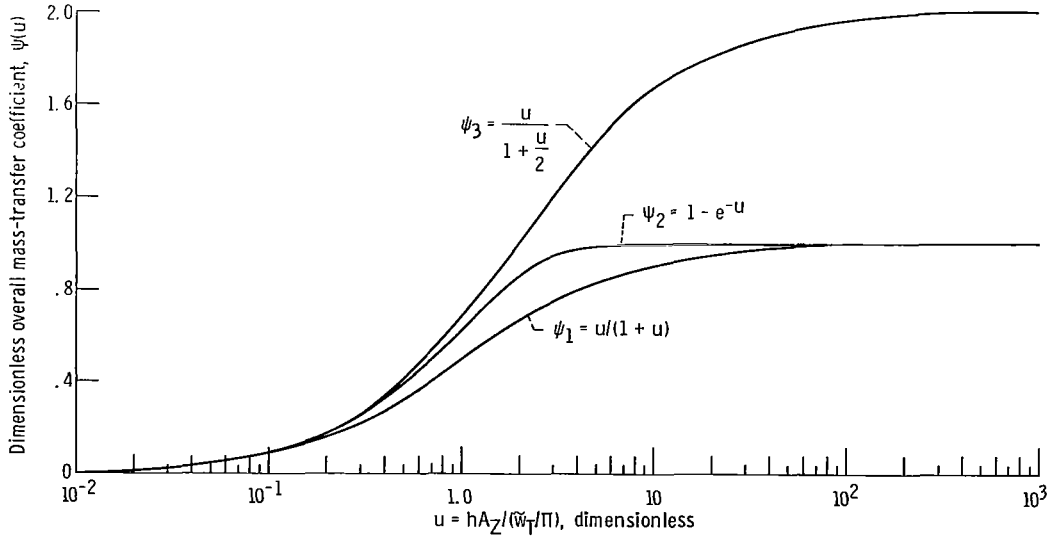

Figure 9. - Form of the dimensionless overall mass-transfer coefficient.

This determination may be made as follows: Two experimental transients are required, of the sort shown in figure 6. (Based on data from ref. 2.) These data in effect illustrate differences in $\tilde{w}_s/\tilde{w}_T$ due to different initial conditions - the high inlet stream humidity corresponding to a relatively dilute electrolyte or "wet" condition and the low humidity to a concentrated electrolyte or "dry" condition. The wet and dry conditions, in turn, may be identified with smaller and larger reaction zone thicknesses, or agglomerate heights (Z_H), respectively. Since h_1 is proportional to Z_H while h_2 is proportional to $1/Z_H$, if h_1 is the correct form for the cell in question, then $\tilde{w}_s$ should be generally greater for the transient with the dryer initial condition. Conversely, if h_2 behavior is controlling, $\tilde{w}_s$ should be greater during the transient having the wetter initial condition. The sense of the word "greater" is evident from figure 6, which indicates that the cell of reference 2 behaves in the fashion described by h_1; that is, the controlling GFHR transport resistance is associated with the gas-liquid interface. The h_1 form for h was, in fact, used in all simulations of reference 2 data.

The quantities in h_2 may a priori be assigned numerical values (the calculation of geometric parameters associated with the flooded agglomerates will be discussed later), but the interfacial mass-transfer coefficient k_i that appears in h_1 is difficult to estimate from theory (although it should not vary during a transient). Because of this fact it was necessary, when simulating the data of reference 2, to use the analog computer simulation to calculate the initial steady-state value of $\psi(u)$. This was accomplished by putting the computer into operation without introducing a perturbation function into the program. Under these conditions the computer was made to calculate the pretransient initial steady-state value of ψ, which, in turn, fixed the value of k_i since k_i is constant throughout a transient.

A second feature of figure 9 is that ψ_1, ψ_2, and ψ_3 become identical for small values of u. More particularly for $u < 10^{-1}$, $\psi_1 = \psi_2 = \psi_3 \simeq u$. Thus, for a cell with poor GFHR transport and a high gas-stream flow rate w_s becomes independent of degree of mixing in the gas cavity and of vapor pressure gradients.

It is also obvious that for $u > 10^2$ $\psi(u)$ becomes independent of u. The dynamic behavior of the cell thus becomes linear if good GFHR transport is coupled with low gas flow rates. It can be seen that this corresponds to equilibrium between the exiting gas and the liquid at the exit.

A final feature of figure 9 is that the ψ dependency on u is readily linearized over small ranges of u. It is easily shown that over any range of u where

$$(u_{max} - u_{min}) << 1$$

the following linear approximations may be made:

$$\psi_1 \simeq \left(\frac{1}{1 + u_{initial}}\right)^2 u$$

$$\psi_2 \simeq e^{-u_{initial}} u$$

$$\psi_3 \simeq \left(\frac{1}{1 + \frac{u_{initial}}{2}}\right)^2 u$$

This linearization simplifies calculations considerably, since the technique may be applied - that of letting the programmed model calculate ψ values based on initial conditions. It was, in fact, found that the linearized form could be used to simulate all the data from reference 2. Note that, if ψ may be linearized and if the model is programmed to calculate initial condition ψ's, then it is unnecessary to decide which form of ψ pertains; that is, details of gas cavity flow and vapor pressure distribution become unnecessary.

The following expression, then, may hold in many cases, regardless of details on cell design:

$$\tilde{w}_s = c \cdot h \cdot (\bar{P}^* - P_{s,i})$$

where c is a coefficient dependent on initial conditions only and all nonlinear behavior of w_s is centered in h, which, in turn, reflects changing agglomerate geometry.

Taking advantage of the relation

$$\theta = \frac{A_{Z\text{-}H_2}}{A_Z Z_H}$$

allows u to be written for $h \equiv h_1$ as

$$u = \frac{A_{Z\text{-}H_2} k_i}{\frac{\tilde{w}_T}{\Pi}}$$

where A_{Z-H_2} is the total agglomerate surface area.

The form of w_s used to simulate the data of reference 2 may now be written:

$$w_s = 18w_s = CA_{Z-H_2}(P^* - P_{s,i}) \tag{A15}$$

Here, again, C is a coefficient generated by the programmed model for each pretransient initial condition.

Calculation of Geometric Parameters

The agglomerate surface area is given by

$$A_{Z-H_2} = A_Z N\Pi r_o^2 + A_Z N2\Pi r_o Z_H$$

in which $A_Z N\Pi r_o^2$ represents the total base area of the agglomerate cylinders abutting the gas chamber and $A_Z N2\Pi r_o Z_H$ the total lateral area. The number of agglomerates per square centimeter of electrode N was calculated from the agglomerate model definition of macroporosity (percentage of electrode not occupied by agglomerates). The equations used to define this void percentage are

$$\varphi = 1 - \frac{w}{\rho H(1 - \epsilon)}$$

and

$$\varphi = 1 - N\Pi r_o^2$$

By equating these two expressions and solving for N, a value of 1.64×10^7 cylinders per square centimeter was determined, and with this the area was calculated to be

$$A_{Z-H_2} = (1.7 + 1300\ Z_H)\text{cm}^2$$

In the programmed model, the calculation of the agglomerate height, Z_H is based on a knowledge of the water and potassium hydroxide masses in the bulk transport zone at any instant of time. The model equations provide continuous calculations of the water mass and the OH^- component of the bulk zone electrolyte. To determine from the OH^-

mass calculation the amount of KOH present at any time, the assumption of electrolyte electroneutrality (ref. 5) was employed. This approximation is based on the fact that the ionic species contained in an electrolytic solution, such as that in the cell being modeled, have sufficient mobility to effectively neutralize the charge at any point within the solution. In terms of the model this defines the molar concentration of K^+ and OH^- of any transport zone to be equal. Therefore, for the bulk transport zone

$$\frac{M_{OH^-\text{-}B}}{17V_B} = \frac{M_{K^+\text{-}B}}{39V_B} \tag{A16}$$

and thus the bulk zone KOH mass is

$$M_{KOH\text{-}B} = M_{K^+\text{-}B} + M_{OH^-\text{-}B} = \left(\frac{39}{17} + 1\right) M_{OH^-\text{-}B} \tag{A17}$$

The water and KOH mass values are then used to determine the bulk zone weight fraction X_{KOH} and hence the bulk mixture density from the empirical relation

$$\rho_E = 0.950 + 1.045\, X_{KOH}$$

The data used in deriving this expression are presented in reference 6. The bulk zone density and liquid-mass composition define the bulk liquid volume from which the bulk zone thickness is calculated to be

$$Z_B = \frac{V_B}{A_Z P}$$

where P is the bulk zone mean porosity. By subtracting Z_B from the total thickness of the electrode-matrix structure, the sum of the heights in the nonflooded portions of the two electrodes is obtained. The nonflooded portion of each electrode Z_H is one-half of this sum, since the bulk electrolyte volume that extends into the electrodes is assumed to be distributed equally between them.

Thus, through the agglomerate-height, electrolyte-volume relation, the area calculation becomes functionally related to the component water and KOH masses of the electrolyte. In terms of the analysis this represents an equation coefficient $A_{Z\text{-}H_2}$, which is a function of the dependent variables of the describing equations; hence a nonlinearity is introduced. In the model this accounts for part of the nonlinear characteristic that

was produced experimentally by varying the preload-step-transient inlet stream humidity (fig. 6); that is, a variation in inlet stream vapor pressure (inlet hydrogen stream humidity) produces a change in the mass composition or electrolyte volume, which, in turn, is reflected into the value of the area $A_{Z\text{-}H_2}$.

DERIVATION OF RATE EXPRESSION FOR DIFFUSION OF WATER INTO THE BULK LIQUID

In the general hydrogen reaction zone continuity equation (eq. (A1)), the expression defining the flow of water from the reaction zone into the bulk zone $w_{E\text{-}H_2}$ is defined by Fick's law. However, Fick's law in this case is applied to mass transport in the liquid state. The equation is

$$-w_{E\text{-}H_2} = \overline{D}_{H_2O\text{-}KOH} A_Z \frac{d\rho_{H_2O}}{dz} \tag{A18}$$

On a lumped parameter basis this is expressed as

$$w_{E\text{-}H_2} = \overline{D}_{H_2O\text{-}KOH} A_Z \left(\frac{\frac{M_{H_2O\text{-}H_2}}{V_{H_2}} - \frac{M_{H_2O\text{-}B}}{V_B}}{\frac{Z_B}{2}} \right) \tag{A19}$$

in which the driving force is the concentration or density difference between the reaction zone electrolyte and the bulk electrolyte. Assuming that no diffusion takes place within the reaction zone, the average diffusive path length is one-half the thickness of the bulk zone ($Z_B/2$). The densities in equation (A19) were calculated from a knowledge of the instantaneous zonal masses and their corresponding calculated volumes. The bulk volume and corresponding thickness Z_B were calculated as outlined; the reaction zone volumes V_{H_2} and V_{O_2}, which are assumed to be equal, were taken to be the instantaneous volumetric sum of their respective reaction-zone agglomerate cylinders.

The diffusion under consideration in equation (A19) takes place in a zone that is made up of both flooded electrode and matrix. For an assumed idealized pore structure, the development presented in reference 7 indicates that the tortuosity τ is defined by the following function,

$$\tau = \frac{3(1 - \alpha)}{\Pi}\left(\frac{\Gamma}{\beta} + 1\right)^2$$

In this expression α is the structure porosity and Γ/β the ratio of effective pore radius to solid fiber radius. By approximating the pore to solid radius ratio to be 2.0 for both portions of the zone, tortuosity factors of 1.05 for the electrode and 5.0 for the matrix portions were obtained from reference 7. These data are presented as a family of linear characteristics that identify the tortuosity as being inversely proportional to structure porosity for various pore-radius to solid-radius ratios. Because of this difference in tortuosities between the two sections of the bulk zone, the net tortuosity of the whole zone changes as the zonal volume varies. In the model this variable tortuosity is accounted for in the diffusion coefficient $\overline{D}_{H_2O\text{-}KOH}$. In particular, the individual tortuosities are treated as factors by which the liquid diffusivity $D_{H_2O\text{-}KOH}$ is divided to obtain the individual effective diffusivities for mass transport through the electrode and matrix portions of the zone. From these two values a weighted mean diffusivity $\overline{D}_{H_2O\text{-}KOH}$ is determined for the overall zone; the weighting factor is determined from the instantaneous relative volumes of the electrode and matrix that constitute the bulk zone.

Relating the zonal diffusivity to the time varying electrolyte volume in this manner represents the introduction of a system nonlinearity, which, along with the variable mass-transfer area, accounts for the experimentally observed, inlet humidity, nonlinear effect (fig. 6).

THE GENERATION TERM

The water generation rate w_R is represented in the basic conservation equation (eq. (A1)) by $1.87\times10^{-7}(I)$ where the quantity 1.87×10^{-7} kilograms per ampere per second is the Faraday constant.

Therefore, as programmed for computer solution, the continuity equation for water in the hydrogen reaction zone is given by

$$\frac{dM_{H_2O\text{-}H_2}}{dt} = 1.87\times10^{-7}(I) - CA_{Z\text{-}H_2}(\overline{P}^* - P_{s,i}) - D_{H_2O\text{-}KOH}A_Z\left(\frac{\frac{M_{H_2O\text{-}H_2}}{V_{H_2}} - \frac{M_{H_2O\text{-}B}}{V_B}}{\frac{Z_B}{2}}\right) \quad \text{(A20)}$$

CONTINUITY EQUATION FOR WATER IN BULK ELECTROLYTE ZONE

The general continuity equation for the bulk zone is

$$\frac{dM_{H_2O\text{-}B}}{dt} = w_{E\text{-}H_2} - w_{E\text{-}O_2}$$

where $w_{E\text{-}H_2}$ represents the flow of water entering from the hydrogen reaction zone and $w_{E\text{-}O_2}$ the flow exiting the bulk zone and entering the oxygen reaction zone. The expression for the flow from the hydrogen reaction zone into the bulk zone $w_{E\text{-}H_2}$ was developed for the hydrogen reaction zone conservation equation and is given by equation (A19).

In applying Ficks' law to obtain $w_{E\text{-}O_2}$, the driving force, which is the density difference between the bulk and oxygen zones, is the only parameter different from the expression for $w_{E\text{-}H_2}$. Therefore, the expression for $w_{E\text{-}O_2}$ can be written directly as

$$w_{E\text{-}O_2} = \bar{D}_{H_2O\text{-}KOH} A_Z \left(\frac{\frac{M_{H_2O\text{-}B}}{V_B} - \frac{M_{H_2O\text{-}O_2}}{V_{O_2}}}{\frac{Z_B}{2}} \right) \tag{A21}$$

and the equation in programmed form is

$$\frac{dM_{H_2O\text{-}B}}{dt} = \bar{D}_{H_2O\text{-}KOH} A_Z \left(\frac{\frac{M_{H_2O\text{-}H_2}}{V_{H_2}} - \frac{M_{H_2O\text{-}B}}{V_B}}{\frac{Z_B}{2}} \right) - \bar{D}_{H_2O\text{-}KOH} A_Z \left(\frac{\frac{M_{H_2O\text{-}B}}{V_B} - \frac{M_{H_2O\text{-}O_2}}{V_{O_2}}}{\frac{Z_B}{2}} \right) \tag{A22}$$

CONTINUITY EQUATION FOR WATER IN THE OXYGEN REACTION ZONE

The general conservation equation for the oxygen zone is given as

$$\frac{dM_{H_2O\text{-}O_2}}{dt} = w_{E\text{-}O_2} - 0.935\times10^{-7}(I) \qquad (A23)$$

In this expression $w_{E\text{-}O_2}$ represents the flow of water entering the oxygen zone from the bulk zone, and $0.935\times10^{-7}(I)$ the rate at which water is consumed by the oxygen-side reaction. The flow term $w_{E\text{-}O_2}$ is defined by equations (A21), and the numerical coefficient on the sink term (0.935×10^{-7}) is the Faraday constant. By applying the flooded agglomerate reaction zone concept and the ensuing assumptions as enumerated for the hydrogen reaction zone, the programmed form of the equation is given as

$$\frac{dM_{H_2O\text{-}O_2}}{dt} = \overline{D}_{H_2O\text{-}KOH} A_Z \left(\frac{\frac{M_{H_2O\text{-}B}}{V_B} - \frac{M_{H_2O\text{-}O_2}}{V_{O_2}}}{\frac{Z_B}{2}} \right) - 0.935\times10^{-7}(I) \qquad (A24)$$

CONTINUITY EQUATION FOR OH^- IN THE HYDROGEN REACTION ZONE

As in the case of water movement, the transport of hydroxide ions dictated by the cell reactions can be mathematically simulated by the continuity equation. For the hydrogen zone it can be expressed as

$$\frac{dM_{OH^-\text{-}H_2}}{dt} = w_{RZ} - 1.78\times10^{-7}(I) \qquad (A25)$$

where w_{RZ} represents the transport of OH^- ions into the reaction zone and $1.78\times10^{-7}(I)$ the consumption rate of OH^- by the hydrogen reaction. The term defining the flow into the zone w_{RZ} is analogous to the water flow terms outlined in the water continuity equation except that the transport in this case results from ionic migration as well as diffusion.

By assuming dilute solution theory to apply plus the absence of convective transport,

an effective mass-transfer coefficient can be approximated that accounts for both diffusion and ionic migration. The K^+ and OH^- ionic fluxes are defined in a general sense by

$$N_{OH^-} = -\left(D_{OH^-}\right)\frac{dC_{OH}}{dZ} - \left(q_{OH^-}\right)\left(U_{OH^-}\right)F\left(\;'_{OH^-}\right)\frac{de}{dZ} \tag{A26}$$

$$N_{K^+} = -\left(D_{K^+}\right)\frac{dC_K}{dZ} - \left(q_{K^+}\right)\left(U_{K^+}\right)F\left(C_{K^+}\right)\frac{de}{dZ} \tag{A27}$$

The first term to the right of the equal sign in each equation, Ficks' law, defines the ionic movement due to diffusion, and the second term defines the ionic movement due to electrical migration. Since the potassium does not enter into the electrode reactions, it can be assumed that the flux of potassium ions N_{K^+} is equal to zero; therefore, equation (A27) can be solved for the potential gradient de/dZ in terms of the parameters that appear in equation (A26). By substituting this expression for potential gradient into equation (A26), the OH^- flux equation becomes

$$N_{OH^-} = -\left(D_{OH^-} + \frac{U_{OH^-}}{U_{K^+}} D_{K^+}\right)\frac{dC_{OH}}{dZ}$$

By the assumption of infinite dilution, which is inherent in the ideal solution approach, the ionic mobilities are defined by the Nernst-Einstein equation to be

$$U_{OH^-} = \frac{D_{OH^-}}{RT}$$

and

$$U_{K^+} = \frac{D_{K^+}}{RT}$$

Substituting these relations into the expression for N_{OH^-} determines the effective mass-transport coefficient D' to be $2D_{OH^-}$. To a first approximation, the value

of D_{OH} may be represented by the value of $D_{H_2O\text{-}KOH}$, binary diffusivity for the H_2O-KOH system.

The transport equation for the movement of OH^- in the hydrogen reaction zone can be expressed as

$$\frac{dM_{OH^-\text{-}H_2}}{dt} = D'A_Z\left(\frac{\frac{M_{OH^-\text{-}B}}{V_B} - \frac{M_{OH^-\text{-}H_2}}{V_{H_2}}}{\frac{Z_B}{2}}\right) - 1.78\times10^{-7}(I) \qquad \text{(A28)}$$

CONTINUITY EQUATION FOR OH^- IN THE BULK AND OXYGEN REACTION ZONES

Except for the difference in parameter values and driving force densities, this equation is analogous to the continuity equation for water in the bulk zone and can be written directly as

$$\frac{dM_{OH^-\text{-}B}}{dt} = D'A_Z\left(\frac{\frac{M_{OH^-\text{-}O_2}}{V_{O_2}} - \frac{M_{OH^-\text{-}B}}{V_B}}{\frac{Z_B}{2}}\right) - D'A_Z\left(\frac{\frac{M_{OH^-\text{-}B}}{V_B} - \frac{M_{OH^-\text{-}H_2}}{V_{H_2}}}{\frac{Z_B}{2}}\right) \qquad \text{(A29)}$$

In this equation the mass of OH^- contained in the oxygen reaction zone is determined, not from an independent continuity equation, but from a knowledge of the continuously calculated bulk and hydrogen zone OH^- masses and the mass of pure KOH loaded into the cell at time of construction. Since the initial electrolyte loading was 0.0105 kilogram and since a net removal of KOH is assumed not to occur, the mass of KOH present in the oxygen zone at any instant is

$$M_{KOH\text{-}O_2} = 0.0105 - M_{KOH\text{-}H_2} - M_{KOH\text{-}B}$$

From the assumption of electroneutrality and the accompanying K^+ and OH^- equality, the instantaneous oxygen zone OH^- mass is determined from the preceding expression to be

$$M_{OH^-\text{-}O_2} = \frac{M_{KOH\text{-}O_2}}{\left(\frac{39}{17} + 1\right)} = 0.0032 - M_{OH^-\text{-}H_2} - M_{OH^-\text{-}B}$$

The largest error introduced by the electroneutrality assumption, as it is applied in this analysis, exists during periods of transient operation. However, the approximation is justified during these periods by the fact that the ionic mobility is such that the realinement to neutrality is fast when compared to the transport transients.

TRANSIENT TEMPERATURE EFFECTS

In the type of cell under consideration, the effect that temperature has on the transport of water is manifest through the temperature-sensitive electrolyte vapor pressure. This sensitivity of vapor pressure to temperature is illustrated in figure 10 in which

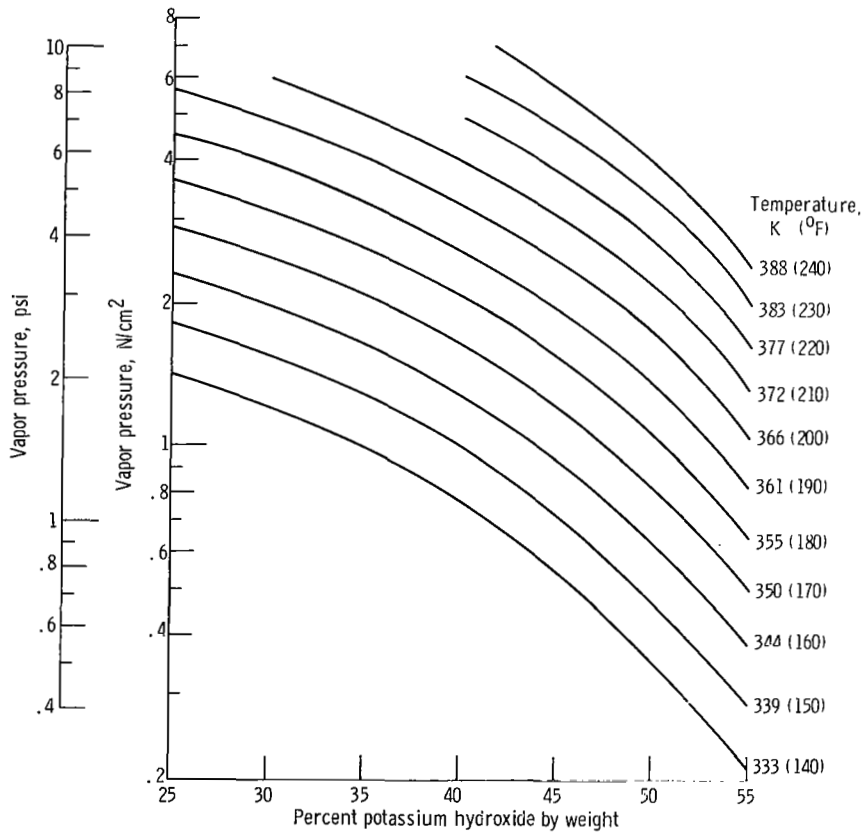

Figure 10. - Vapor pressure of aqueous potassium hydroxide as function of weight percent potassium hydroxide (ref. 8).

vapor pressure is plotted against weight-percent of KOH for a range of temperature values.

In terms of water transport, a transient temperature increase that accompanies a load step produces an increase in electrolyte vapor pressure and hence an effective increase in the force driving water into the reactant stream. Therefore, unless compensated for by other cell operating parameters, an increase in cell temperature has a drying effect on a cell.

Since in the model the cell thermal response accompanying a step in load was not simulated analytically, experimental thermal transient data that were taken were used to calculate the time varying temperature effect any particular load transient had on the electrolyte vapor pressure. By knowing the approximate initial electrolyte concentration and cell temperature, a transient change in vapor pressure resulting from a transient temperature response was obtained by scaling the data of figure 10 for temperature and picking off data points to correspond to the data points of the time varying temperature. However, since the electrolyte weight fraction changes during any load transient, the vapor pressure data could not be taken off a constant weight fraction line in figure 10. To account for this fact in the model, an approximation for the final, posttransient concentration was determined and the data points were picked off a straight line struck between the initial and final concentrations.

The transient vapor pressure increase resulting from the temperature transient accompanying a 40-ampere load step is shown in figure 11. The actual temperature cor-

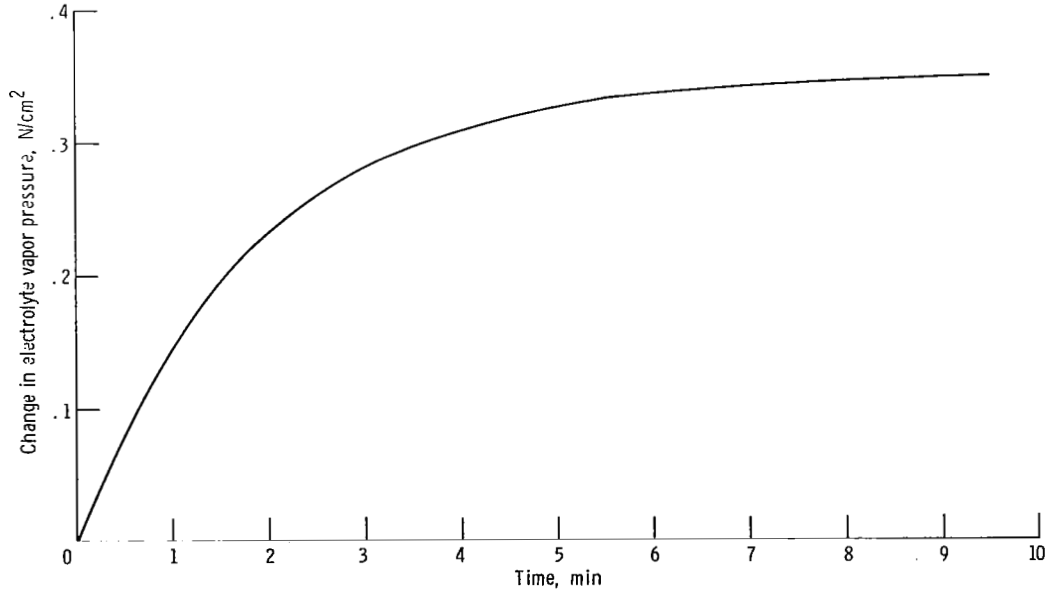

Figure 11. - Temperature effect on electrolyte vapor pressure for 40-ampere load step. Operating conditions: current step, 20 to 60 amperes; inlet stream hydrogen content, 0.05 kilogram per hour (0.12 lb/hr); water content, of inlet stream, 0.05 kilogram per hour (0.12 lb/hr).

rection was made by adding the time varying vapor pressure change of figure 11 to $\overline{P}^*$, the reaction zone electrolyte vapor pressure, as the model was responding the 40-ampere step change.

PERTINENT FUEL CELL PARAMETERS, DIMENSIONS, AND OPERATING CONDITIONS

The following table lists values of pertinent fuel cell parameters, dimensions, and operating conditions.

Measured values

Gas chamber (x direction) cross sectional area, cm^2; $in.^2$	5.23; 2.06
Electrode area, A_Z, cm^2; $in.^2$	213; 33.1
Hydrogen gas chamber length, L, cm; in.	2.21; 0.87
Hydrogen supply chamber thickness, cm; in.	0.152; 0.06
Nominal cell operating temperature, T, K; ^oF	366; 200
Compressed matrix thickness, cm; in.	0.051; 0.02
Catalyst loading, w, kg/cm^2; $lb/in.^2$	4.0×10^{-5}; 5.68×10^{-4}
Catalyst density, ρ, kg/cm^3; $lb/in.^3$	2.01×10^{-2}; 0.724
Electrode thickness, H, cm; in.	0.076; 0.030

Reasonable values obtained from the literature

Mass transport coefficient of OH^- in electrolyte, D', cm^2/sec; $in.^2/sec$	1.8×10^{-4}; 2.8×10^{-5}
Mass diffusivity of water - potassium hydroxide mixture, $D_{H_2O\text{-}KOH}(= 1/2\ D')$, cm^2/sec; $in.^2/sec$	0.90×10^{-4}; 1.4×10^{-5}
Bulk zone mean porosity, P	0.5
Compressed matrix porosity	0.42

Assumed values

Tortuosity of flooded electrode portion of bulk electrolyte zone	1.05
Tortuosity of matrix portion of bulk electrolyte zone	5.0
Agglomerate radius, r_o, cm; in.	0.001; 3.9×10^{-4}
Agglomerate porosity, ϵ	0.50

APPENDIX B

SYMBOLS

A_Z	electrode area, cm^2; $in.^2$
$A_{Z\text{-}H_2}$	hydrogen reaction zone agglomerate surface area, cm^2; $in.^2$
C	linear portion of overall mass-transfer coefficient, cm^2
C_{OH^-}	molar concentration of hydroxide ions in KOH-water mixture, kg-mole/cm^3; lb-mole/$in.^3$
C_{K^+}	molar concentration of potassium ions in KOH-water mixture, kg-mole/cm^3; lb-mole/$in.^3$
D'	mass-transport coefficient of hydroxide ions in cell electrolyte, cm^2/sec; $in.^2$/sec
D_g	diffusion coefficient for $H_2O\text{-}H_2$, cm^2/sec, $in.^2$/sec
$D_{H_2O\text{-}KOH}$	mass diffusivity of KOH-water mixture, cm^2/sec; $in.^2$/sec
$\overline{D}_{H_2O\text{-}KOH}$	weighted mean diffusion coefficient for bulk transport zone, cm^2/sec; $in.^2$/sec
D_{K^+}	diffusivity of potassium ions in KOH-water mixture, cm^2/sec; $in.^2$/sec
D_{OH^-}	diffusivity of hydroxide ions in KOH-water mixture, cm^2/sec; $in.^2$/sec
e	electrostatic potential, V
F	Faraday's constant, C/equiv
H	electrode thickness, cm; in.
h	local mass-transfer coefficient, mole/(cm^2)(sec)(N/cm^2)
h_1	local mass-transfer coefficient of transport interface controlled mole/(cm^2)(sec)(N/cm^2)
h_2	local mass-transfer coefficient of transport diffusion controlled mole/(cm^2)(sec)(N/cm^2)
I	current, A
k_i	gas-liquid interfacial mass-transfer coefficient, mole/(cm^2)(sec)(N/cm^2)
L	hydrogen gas chamber length, cm; in.
ℓ	width of gas flow path in gas cavity, cm; in.

M_{H_2O-B}	mass of water contained in bulk electrolyte zone, kg; lbm
$M_{H_2O-H_2}$	mass of water contained in hydrogen reaction zone, kg; lbm
$M_{H_2O-O_2}$	mass of water contained in oxygen reaction zone, kg; lbm
M_{KOH-B}	mass of pure potassium hydroxide in bulk electrolyte zone, kg; lbm
M_{K^+-B}	mass of potassium ions in bulk electrolyte zone, kg; lbm
$M_{OH^--H_2}$	mass of hydroxide ions in hydrogen reaction zone, kg; lbm
M_{OH^--B}	mass of hydroxide ions in bulk zone kg; lbm
$M_{OH^--O_2}$	mass of hydroxide ions in oxygen reaction zone, kg; lbm
N	number of agglomerate cylinders per cm^2 of electrode
N_{H_2O}	flow rate of H_2O vapor out of electrode per unit electrode geometrical area, mole/(cm^2)(sec)
N'_{H_2O}	flow rate of H_2O in Z-direction per unit gas flow area, mole/(sec)(cm^2)
N_i	flow rate of H_2O into GFHR per unit gas-liquid interface area, mole/(sec)(cm^2)
P^*	local x-dependent electrolyte equilibrium vapor pressure, N/m^2; psi
$\overline{P}^*$	overall mean reaction zone electrolyte vapor pressure N/m^2; psi
$P_{H_2O}(Z)$	partial pressure of H_2O at Z in GFHR, N/m^2; psi
P_s	local H_2O partial pressure in hydrogen supply chamber, N/m^2; $lb/in.^2$
$P_{s,i}$	partial pressure in hydrogen stream at cell inlet, N/m^2; $lb/in.^2$
q_{K^+}	valence of potassium ions
q_{OH^-}	valence of hydroxide ions
R	water vapor gas constant, (cm)(lb)/(kg)(K); in.-lb/(lbm)(R)
r_o	agglomerate radius, cm; in.
T	temperature, K: R
t	time, sec
u	dimensionless parameter, $hA_Z/(\tilde{w}_T/\Pi)$
U_{OH^-}	mobility of OH^- ions, (cm^2)(mole)/(J)(sec); ($in.^2$)(mole)/(in.-lb)(sec)
U_{K^+}	mobility of K^+ ions, (cm^2)(mole)/(J)(sec); ($in.^2$)(mole)/(in.-lb)(sec)

V_B	bulk electrolyte transport zone volume, cm^3; $in.^3$
V_{H_2}	hydrogen reaction zone volume, cm^3; $in.^3$
V_{O_2}	oxygen reaction zone volume, cm^3; $in.^3$
w	catalyst loading, kg/cm^2; $lb/in.^2$
w_{E-H_2}	mass flow of water into bulk electrolyte zone, kg/sec; lb/sec
$\tilde{w}_{H_2O}$	molar flow rate of H_2O in gas cavity, mole/sec
w_k	water generation rate, kg/sec; lb/sec
w_s	mass flow rate of H_2O into gas cavity, kg/sec; lb/sec
$\tilde{w}_s$	molar flow rate of H_2O into gas cavity, kg-mole/sec; lb-mole/sec
$\tilde{w}_T$	total molar flow of gas through gas cavity, kg-mole/sec; lb-mole/sec
X	distance from cell entrance in direction of flow, cm; in.
Z'	distance (in gas phase) from agglomerate base, cm; in.
Z_B	bulk electrolyte transport zone thickness, cm; in.
Z_H	nonflooded portion of each electrode, cm; in.
ϵ	agglomerate microporosity
θ	gas-liquid interface area per unit electrode geometric volume, cm^{-1}; $in.^{-1}$
φ	gas filled cross-sectional area per unit geometrical area, dimensionless
Π	total pressure, N/m^2; psi
ρ	catalyst density, kg/cm^3; $lb/in.^3$
ρ_E	density of KOH-water mixture in bulk electrolyte transport zone, kg/cm^3; $lb/in.^3$
ρ_{H_2O}	density of water in bulk electrolyte, kg/cm^3; $lb/in.^3$
$\psi(u)$	dimensionless overall mass-transfer coefficient
ψ_1, ψ_2, ψ_3	alternate forms of ψ, the dimensionless overall mass-transfer coefficient

REFERENCES

1. Prokopius, Paul R.; and Hagedorn, Norman H.: Investigation of the Dynamics of Water Rejection from a Hydrogen-Oxygen Fuel Cell to a Hydrogen Stream. NASA TN D-4201, 1967.

2. Prokopius, Paul R.; and Easter, Robert W.: Experimental Investigation of the Dynamics of Water Rejection from a Matrix Type of Hydrogen-Oxygen Fuel Cell. NASA TN D-4956, 1968.

3. Giner, J.; and Hunter, C.: The Mechanism of Operation of the Teflon-Bonded Gas Diffusion Electrode: A Mathematical Model. J. Electrochem. Soc., vol. 116, no. 8, Aug. 1969, pp. 1124-1130.

4. Levenspiel, O.: Chemical Reaction Engineering: An Introduction to the Design of Chemical Reactors. John Wiley & Sons, Inc., 1962.

5. Newman, John: Transport Processes in Electrolytic Solutions. Advances in Electrochemistry and Electrochemical Engineering. Vol. 5. Charles W. Tobias, ed., John Wiley & Sons, Inc. 1967, pp. 87-137.

6. Walker, Robert D., Jr.: A Study of Gas Solubilities and Transport Properties in Fuel Cell Electrolytes. Florida Univ. (NASA CR-106407), Feb. 25, 1969.

7. Katan, J.: Factors Affecting the Performance of Porous Structures Used as Oxygen Fuel Cell Electrodes. NASA CR-1623, 1970, pp. 132-140.

8. Anon.: Solvay Technical and Engineering Service Bulletin No. 15. First ed., second printing, table 10, p. 26.